ACS APPLIED MATERIALS & INTERFACES

Research Article

www.acsami.org

Evolution of the Electron Mobility in Polymer Solar Cells with Different Fullerene Acceptors

Dong Gao, Brandon Djukic, Weiqing Shi, Colin R. Bridges, Lisa M. Kozycz, and Dwight S. Seferos*

Department of Chemistry, University of Toronto, 80 St. George Street, Toronto, Ontario, M5S 3H6 Canada

Supporting Information

ABSTRACT: We investigate the evolution of the electron mobility of two different acceptors, [6,6]-phenyl C71 butyric acid methyl ester ($PC_{71}BM$) and indene-C60 bisadduct (ICBA), in a poly(3-hexylthiophene) blend solar cell during a prolonged thermal aging process. High electron mobility does not correlate with the best device performance in our study of the P3HT:$PC_{71}BM$ and P3HT:ICBA systems. Very little changes are observed in the polymer crystallinity as a function of time. The evolution of the acceptor appears to be the dominant factor that leads to long-term changes in the device performance. The electron mobility evolves differently in $PC_{71}BM$ and ICBA systems, which highlights the importance of the fullerene molecular structure.

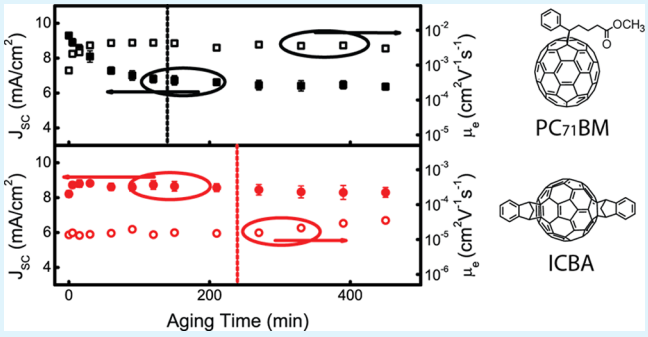

KEYWORDS: *polymer solar cells, evolution, electron mobility, fullerene acceptors*

1. INTRODUCTION

The rapid development of conjugated polymer donor materials has raised the power conversion efficiency (η) to near the theoretical limit of organic solar cells.[1,2] High-efficiency polymer materials should have not only desired energy levels for optimal spectral coverage and voltage output but also ideal structural properties, such as crystallinity and the ability to mix with the acceptor material, which further determines the charge-generation and charge-transport processes.[3] In contrast to the rapid development of conjugated polymer donor materials,[2,4−11] the fullerene-based acceptors [6,6]-phenyl C61 butyric acid methyl ester ($PC_{61}BM$) and [6,6]-phenyl C71 butyric acid methyl ester ($PC_{71}BM$) remain the cornerstone of all high-efficiency bulk-heterojunction solar cells. Recent work has focused on the development of alternative fullerene derivates to PCBM with higher-lying lowest unoccupied molecular orbital (LUMO) levels and therefore larger open-circuit voltages (V_{oc}). However, few alternatives work as well as PCBM in the context of a device. Polymer−fullerene blends are not a simple network of two pure materials but also include miscible two-component regions.[12−14] Several studies have suggested that the chemical nature of the fullerene acceptor is very important to blend morphology.[15−17] How the structure and properties of the fullerene relate to the structure and properties of the device is not well understood.

For the best device efficiency, the optimal morphology of polymer−fullerene is prepared empirically, typically requires thermal annealing, and results in the formation of a kinetic product. Extending the length of the thermal annealing process beyond what is optimal will result in the overgrowth of fullerene domains, leading to a loss in the device performance. It is important to note that the structure of the fullerene not only affects its LUMO level but also plays an important role in its crystallinity. Understanding the dynamic role of fullerene is important not only for the achievement of optimal device performance but also for the stability of the blend, which is ultimately related to the device lifetime.

Herein we study the evolution of electron mobility of polymer solar cells composed of poly(3-hexylthiophene) (P3HT)/$PC_{71}BM$ as well as P3HT/indene-C60 bisadduct (ICBA). ICBA has a high-lying LUMO level that results in a high voltage and good efficiency when blended with P3HT.[18,19] However, ICBA is less crystalline than PCBM.[20] Because the charge-carrier mobility governs both extraction and recombination of charge carriers for active blends,[21,22] it is rational to assume that improving the mobility will improve the device performance; however, little work has been presented on the evolution of the charge-carrier mobility and its effect on the photovoltaic behavior. Furthermore, because of the competition between fullerene and polymer morphology evolution, it is difficult to distinguish these two effects based purely on the photovoltaic behavior. Therefore, in this work, we monitor the evolution of the electron mobility, in addition to the device performance. Polymer crystallinity, optical absorption properties, electron mobility, topography, and device performance parameters were also evaluated. A 2-day accelerated aging process was carried out to follow the dynamic evolution of the polymer−fullerene blends comprising the devices.

Received: June 3, 2013
Accepted: July 11, 2013
Published: July 11, 2013

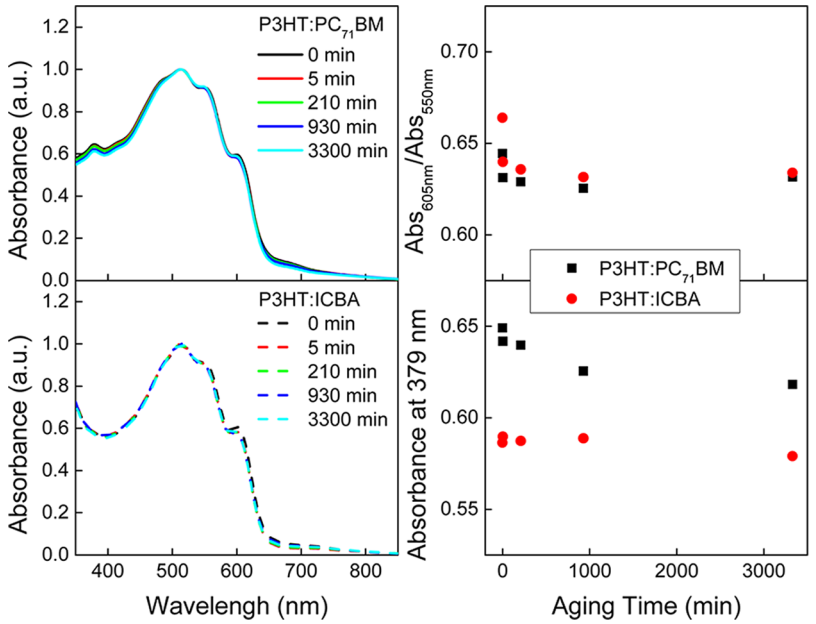

Figure 1. Optical absorption spectra of P3HT:PCBM (solid line) and P3HT:ICBA (dashed line) films after aging at 100 °C for the amount of time indicated.

2. EXPERIMENTAL SECTION

P3HT (Rieke Metals), $PC_{71}BM$ (American Dye Source), and ICBA (Solaris) were purchased and used as received. Devices were fabricated on commercial indium−tin oxide (ITO) substrates (Colorado Concept Coatings) that had a sheet resistance of ∼10 Ω/□. These substrates were cleaned in aqueous detergent, deionized water, acetone, and methanol and subsequently treated in an oxygen-plasma cleaner for 5 min. Next, poly(3,4-ethylenedioxythiophene)/poly-(styrenesulfonate) (PEDOT:PSS; Clevios P VP AI 4083) was coated onto the substrates at 3000 rpm and annealed at 130 °C in air for 15 min, after which the substrates were transferred into a nitrogen-filled glovebox. Both P3HT:ICBA and P3HT:$PC_{71}BM$ films were spin-coated at 800 rpm from 1,2-dichlorobenzene solutions (20:20 mg/mL). The solutions were stirred at 50 °C overnight before spin-coating to ensure complete dissolution. Immediately after deposition, the substrates were transferred into sealed Petri dishes (while the films were wet) and allowed to slowly dry at room temperature. This procedure is the so-called vapor-annealing process and has been shown to improve the crystallinity of P3HT.[23−26] Films were left in the glovebox at room temperature for 2 days before subsequent measurements to allow all of the solvent residue to evaporate. The film thickness is 110 nm. To finish the device, a 0.8 nm LiF layer and a 100 nm Al cathode were thermally deposited through a shadow mask at ∼10^{-6} Torr using an Angstrom Engineering Covap II (Kitchener, Ontario, Canada). The device area is 0.07 cm^2, as defined by the area of the circular Al cathode. *I*−*V* characteristics were measured using a Keithley 2400 source meter under simulated AM 1.5 G condition. The mismatch of the simulator spectrum was calibrated using a Si diode with a KG-5 filter. External quantum efficiency spectra were recorded and compared with a Si reference cell that is traceable to the National Institute of Standards and Technology. Electron-only single-carrier devices were fabricated in an analogous manner with the structure of ITO/Al/P3HT:acceptor/LiF/Al. Current (*I*)−voltage (*V*) characteristics of the single-carrier devices were measured under dark conditions, and the mobility was estimated from the Mott−Gurney law.

The accelerated aging process was carried out on a hot plate inside the glovebox that was maintained at 100 °C. This temperature is lower than the typical thermal annealing temperature for device optimization. We selected this temperature because it is expected to accelerate the dynamic evolution of the blend.[27,28] The slower diffusion of fullerene molecules at low heating temperature allows us to distinguish the influence of acceptor morphology evolution on device performances without the influence of polymer crystallization.

Optical absorption spectra were recorded using a Varian Cary 5000 UV−vis−IR spectrophotometer. For this measurement blends were spin-coated onto glass substrates using the same conditions as those of the devices. Grazing incidence X-ray diffraction (GIXRD) data were collected on a Bruker D8 Discover with a Co-sealed tube source, parallel beam optics, a $^1/_4\chi$ cradle, and a Vantec500 area detector. The hot stage was an Anton Paar DHS 900 with a TCU 150 temperature control unit. The dome surrounding the sample is made of PEEK [a synthetic material based on a poly(ether ether ketone) resin]. XRD2 frames were integrated using Bruker Pilot software (v2011.4-0). Peak positions were found using the Bruker Topas software (version 4.2).

3. RESULTS AND DISCUSSION

Optical absorption spectroscopy was used to examine the absorption profile of the two fullerene/P3HT blends as a function of time. The absorption spectra are normalized to account for any differences in the film thickness (Figure 1). The A_{0-0} (605 nm)/A_{0-1} (550 nm) ratio is used to evaluate the crystallinity of P3HT.[29−31] Both samples have a slightly larger A_{0-0} shoulder and a greater A_{0-0}/A_{0-1} ratio before aging. The A_{0-0}/A_{0-1} ratio changes only at the beginning and not during the latter stages of the aging process. This indicates that the polymer organization is nearly complete after the vapor annealing process. On the other hand, the peaks associated with fullerene absorption decrease gradually during the entire 2-day aging process. The $PC_{71}BM$ absorption peak (∼379 nm) decreases to a greater extent than ICBA absorption at the same wavelength. These observations are likely the result of the formation of larger crystalline regions, which scatter rather than absorb light. Although it is not possible to detect the formation of nanometer-sized molecular regions using this optical analysis, it appears that $PC_{71}BM$ crystallizes more rapidly than ICBA within the P3HT matrix. The crystallization behavior of the fullerene should influence the electron mobility, the blend structure, and likely the stability of the donor−acceptor interface within the blend.

Temperature-dependent XRD was used to further investigate the structures of the P3HT:$PC_{71}BM$ and P3HT:ICBA blend films. The patterns (Figures 2 and S1 in the Supporting Information) were used to determine the interchain spacing (or *d* spacing) of P3HT chains before, during, and after accelerated aging. Prior to aging, both samples have 16.1 Å *d* spacings, which is the same as that of the neat P3HT film.[32] The spacing rapidly increases to 17.4 Å at 100 °C, showing that the P3HT lamellae swell at higher temperature. If the sample is then cooled after 10 min, the *d* spacing contracts to 16.6 Å for the P3HT:ICBA sample and 16.8 Å for the P3HT:$PC_{71}BM$ sample. Interestingly, the *d* spacings of the cooled samples are identical if they are heated for 10 min or 2 days. The larger spacing may be indicative of improved ordering of the alkyl chains.[33] The fact that the spacing does not change after extended aging indicates than any improvements in P3HT occur relatively rapidly. The intensity and full width at half-maximum of the peaks are also similar, indicating similar polymer crystallinity during the aging process. The differential scanning calorimetry (DSC) thermograms show consistent results as well (Figure S2 in the Supporting Information). The crystallinity of the polymer does not appear to be significantly affected by the different acceptors. When measuring the device performance, we find that the open-circuit voltage (V_{oc}) increases at the stages of accelerated aging that coincide with an increase in *d* spacing (Table 1). On the basis of these observations and the optical spectroscopy presented above, it appears that the polymer crystallinity only changes in the beginning of the experiment and evolves very little thereafter. On the other hand, the fullerene crystallinity appears to evolve much more slowly.

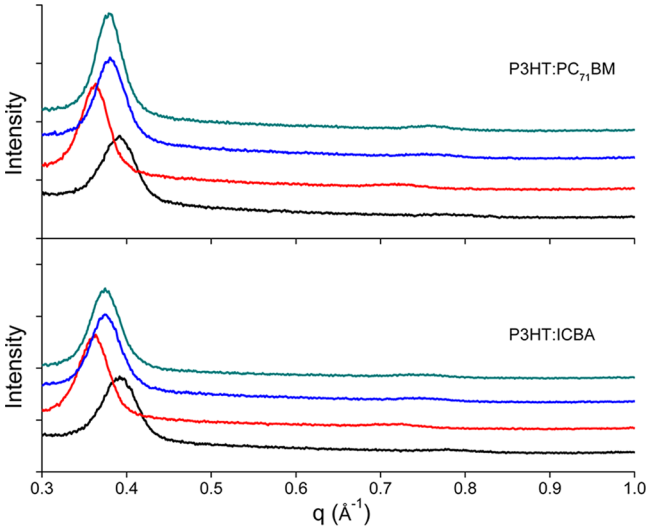

Figure 2. XRD patterns of P3HT:$PC_{71}BM$ (above) and P3HT:ICBA (below) films before aging (black), during aging at 100 °C (red), and cooled after aging for 10 min (blue) or 2 days (cyan).

To investigate the influence of fullerene crystallinity evolution, we next compare the electron mobility and device short-circuit current (J_{sc}) as a function of accelerated aging (Figure 3). Because a crystalline region has higher charge-carrier mobility than an amorphous region[34] and electrons mainly transfer through the n-type fullerene molecules, the electron mobility can be correlated with the fullerene crystallinity. The electron mobility was extracted from single-carrier *I*–*V* measurements. Strikingly, the initial electron mobility of the P3HT:$PC_{71}BM$ film is over 1 order of magnitude greater than that of the P3HT:ICBA film. This could be, in part, caused by the lower crystallinity of ICBA compared with $PC_{71}BM$. This also appears to correlate with a lower fill factor (FF) for P3HT:ICBA relative to P3HT:$PC_{71}BM$.

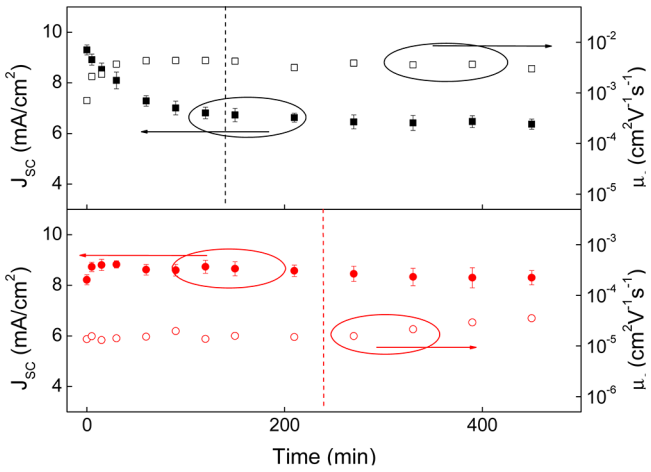

Figure 3. Electron mobility and short-circuit current of P3HT:$PC_{71}BM$ (above) and P3HT:ICBA (below) as a function of the aging time at 100 °C.

During the aging process, the electron mobility of P3HT:$PC_{71}BM$ reaches a maximum value after around 120 min, and only slightly decreases at very long times. On the other hand, the electron mobility of P3HT:ICBA increases very slowly as a function of time. This result is consistent with optical absorption spectroscopy, which also suggests a slower evolution of ICBA molecules. The fast rise in the P3HT:$PC_{71}BM$ sample electron mobility can be assigned to

Table 1. Device Parameters at Different Aging Times[a]

	aging time (min)	J_{sc} (mA/cm^2)	V_{oc} (V)	FF (%)	η (%)
P3HT:$PC_{71}BM$	0	9.30 (±0.19)	0.60 (±0.00)	62.78 (±1.01)	3.50 (±0.08)
	5	8.91 (±0.22)	0.60 (±0.00)	59.26 (±0.63)	3.17 (±0.11)
	450	6.37 (±0.20)	0.60 (±0.00)	59.41 (±0.66)	2.27 (±0.08)
	3330	6.21 (±0.18)	0.56 (±0.01)	56.07 (±1.33)	1.96 (±0.10)
P3HT:ICBA	0	8.22 (±0.20)	0.74 (±0.01)	54.40 (±0.62)	3.32 (±0.07)
	5	8.73 (±0.19)	0.80 (±0.00)	56.82 (±0.54)	3.97 (±0.07)
	450	8.30 (±0.28)	0.81 (±0.01)	52.85 (±0.72)	3.55 (±0.15)
	3330	5.61 (±0.18)	0.79 (±0.01)	46.99 (±0.77)	2.08 (±0.07)

[a]The standard deviation is from eight individual devices.

dx.doi.org/10.1021/am402100f | ACS Appl. Mater. Interfaces 2013, 5, 8038–8043

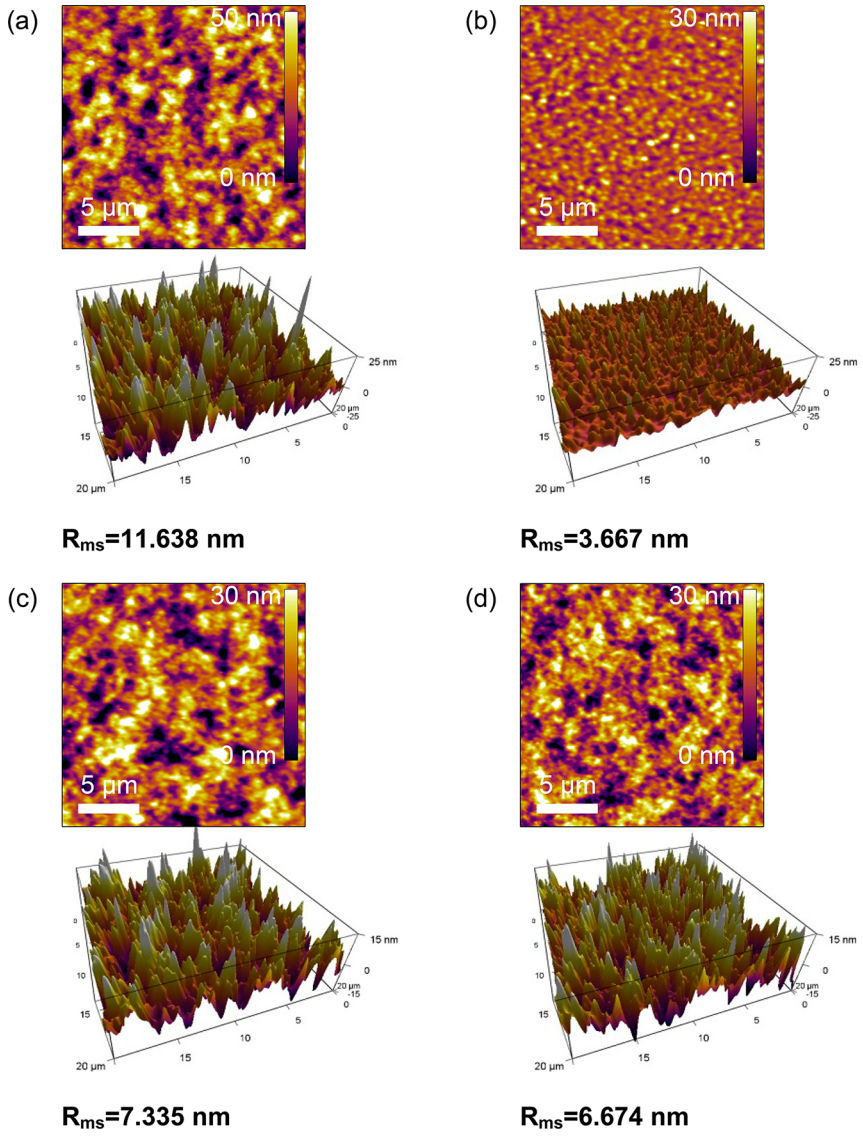

Figure 4. AFM topography images of P3HT:$PC_{71}BM$ (a and b) and P3HT:ICBA (c and d) blend films before (a and c) and after (b and d) aging at 100 °C for 2 days.

increasing $PC_{71}BM$ crystallinity.[35] Under the low heating temperature that we used for accelerated aging, the increased crystallinity is attributed to the growth of existing regions rather than the formation of new regions.[35,36] The diffusion-controlled growth of crystalline $PC_{71}BM$ regions will first increase the overall electron mobility but eventually depletes free $PC_{71}BM$ molecules from a nearby region, which facilitates charge transport between crystalline $PC_{71}BM$ regions. The mechanism is similar for the P3HT:ICBA sample; however, because there is less driving force for crystallization, morphology evolution is much slower than that for $PC_{71}BM$, and we never reach a point where the electron mobility decreases in ICBA.

Interestingly, when considering the electron mobility and J_{sc} together, they are inversely correlated; when the electron mobility increases, J_{sc} decreases in both blends. Moreover, given that both blends use the same polymer and P3HT:ICBA and P3HT:$PC_{71}BM$ have very different electron mobilities, it appears that P3HT has a high tolerance to changes in the electron mobility when the morphology is optimized. Taken together, this behavior suggests that increasing the sizes of the crystalline fullerene regions has a negative effect on the device performance, which is most likely due to the reduced area of the donor−acceptor interfaces, and this offsets any improvements in the electron mobility of the acceptor.

The evolution of surface morphology before and after aging was investigated by atomic force microscopy (AFM; Figure 4). The surface of the P3HT:$PC_{71}BM$ film is much smoother after aging for 2 days, which may lead to poor contact to the top cathode, as observed by the decrease in V_{oc} (Figure S3 in the Supporting Information). The smoother surface of the P3HT:$PC_{71}BM$ film could be caused by migration of the $PC_{71}BM$ molecules in the amorphous P3HT to the large fullerene domains in the $PC_{71}BM$-rich bottom region, which make the amorphous P3HT near the surface smoother. On the other hand, the P3HT:ICBA films change very little. Although the surface topologies are different from those for the P3HT:$PC_{71}BM$ and P3HT:ICBA films, the enlarged images show that the packings of the polymer lamellae are very similar (Figure S4 in the Supporting Information). The difference in the surface morphology evolution is consistent with the slower evolution of ICBA relative to $PC_{71}BM$.

dx.doi.org/10.1021/am402100f | ACS Appl. Mater. Interfaces 2013, 5, 8038−8043

4. CONCLUSIONS

We investigated evolution of the electron mobility of two different acceptors in a crystallized P3HT matrix during a prolonged thermal aging process. ICBA (a superior acceptor with respect to the device performance) has an electron mobility that is over 1 order of magnitude lower than that of $PC_{71}BM$. Given that both devices use the same polymer donor, it appears that high electron mobility does not correlate with the best device performance, as least in our study of both the P3HT:$PC_{71}BM$ and P3HT:ICBA systems. Very few changes are observed in the polymer crystallinity as a function of time. Evolution of the acceptor appears to be the dominant factor that leads to long-term changes in the device performance. The electron mobility evolves differently in the $PC_{71}BM$ and ICBA systems, which highlights the importance of the fullerene molecular structure. Although this work uses a highly crystalline polymer and, for polymers with crystallinities different from that of P3HT, the polymer may evolve as well, it does not appear to be the case here. Our recent work has shown that crystalline block copolymers (P3HS-*b*-P3HT) have improved device stability relative to a crystalline homopolymer (P3HT).[37,38] Phase separation between polymer blocks may eliminate the continued growth of fullerene, resulting in a more stable donor−acceptor morphology. Understanding the evolution of fullerene molecules is important not only for searching for alternative acceptors but also for designing polymer donors with higher performance and better stability.

■ ASSOCIATED CONTENT

Ⓢ Supporting Information

2D XRD patterns, AFM phase images, DSC thermograms of the P3HT:$PC_{71}BM$ and P3HT:ICBA films before and after aging at 100 °C for 2 days, and device parameters as a function of time during accelerated aging. This material is available free of charge via the Internet at http://pubs.acs.org.

■ AUTHOR INFORMATION

Corresponding Author

*E-mail: dseferos@chem.utoronto.ca.

Notes

The authors declare no competing financial interest.

■ ACKNOWLEDGMENTS

This work was supported by the University of Toronto, NSERC, the CFI, and the Ontario Research Fund. D.S.S. is grateful to the Connaught Foundation (Innovation Award), MaRS Innovation (Proof-of-Principle Grant), and DuPont (Young Professor Grant). The authors thank Sean Campbell and Jim Duliban (Angstrom Engineering) for guidance on the evaporation system used in the device evaluation.

■ REFERENCES

(1) Dennler, G.; Scharber, M. C.; Brabec, C. J. *Adv. Mater.* **2009**, *21*, 1323−1338.
(2) He, Z.; Zhong, C.; Su, S.; Xu, M.; Wu, H.; Cao, Y. *Nat. Photonics* **2012**, *6*, 591−595.
(3) Clarke, T. M.; Durrant, J. R. *Chem. Rev.* **2010**, *110*, 6736−6767.
(4) Liang, Y.; Xu, Z.; Xia, J.; Tsai, S.-T.; Wu, Y.; Li, G.; Ray, C.; Yu, L. *Adv. Mater.* **2010**, *22*, E135−E138.
(5) You, J.; Dou, L.; Yoshimura, K.; Kato, T.; Ohya, K.; Moriarty, T.; Emery, K.; Chen, C.-C.; Gao, J.; Li, G.; Yang, Y. *Nat. Commun.* **2013**, *4*, 1446.
(6) Jahnke, A. A.; Seferos, D. S. *Macromol. Rapid Commun.* **2011**, *32*, 943−951.
(7) Hollinger, J.; DiCarmine, P. M.; Karl, D.; Seferos, D. S. *Macromolecules* **2012**, *45*, 3772−3778.
(8) Li, L.; Hollinger, J.; Jahnke, A. A.; Petrov, S.; Seferos, D. S. *Chem. Sci.* **2011**, *2*, 2306−2310.
(9) Kozycz, L. M.; Gao, D.; Hollinger, J.; Seferos, D. S. *Macromolecules* **2012**, *45*, 5823−5832.
(10) Gibson, G. L.; McCormick, T. M.; Seferos, D. S. *J. Am. Chem. Soc.* **2012**, *134*, 539−547.
(11) Hollinger, J.; Sun, J.; Gao, D.; Karl, D.; Seferos, D. S. *Macromol. Rapid Commun.* **2013**, *34*, 437−441.
(12) Mueller, C.; Ferenczi, T. A. M.; Campoy-Quiles, M.; Frost, J. M.; Bradley, D. D. C.; Smith, P.; Stingelin-Stutzmann, N.; Nelson, J.. *Adv. Mater.* **2008**, *20*, 3510−3515.
(13) Collins, B. A.; Gann, E.; Guignard, L.; He, X.; McNeill, C. R.; Ade, H. *J. Phys. Chem. Lett.* **2010**, *1*, 3160−3166.
(14) Jamieson, F. C.; Domingo, E. B.; McCarthy-Ward, T.; Heeney, M.; Stingelin, N.; Durrant, J. R. *Chem. Sci.* **2012**, *3*, 485−492.
(15) Miller, N. C.; Sweetnam, S.; Hoke, E. T.; Gysel, R.; Miller, C. E.; Bartelt, J. A.; Xie, X. X.; Toney, M. F.; McGehee, M. D. *Nano Lett.* **2012**, *12*, 1566−1570.
(16) Guilbert, A. A. Y.; Reynolds, L. X.; Bruno, A.; MacLachlan, A.; King, S. P.; Faist, M. A.; Pires, E.; Macdonald, J. E.; Stingelin, N.; Haque, S. A.; Nelson, J. *ACS Nano* **2012**, *6*, 3868−3875.
(17) Treat, N. D.; Varotto, A.; Takacs, C. J.; Batara, N.; Al-Hashimi, M.; Heeney, M. J.; Heeger, A. J.; Wudl, F.; Hawker, C. J.; Chabinyc, M. L. *J. Am. Chem. Soc.* **2012**, *134*, 15869−15879.
(18) Zhao, G.; He, Y.; Li, Y. *Adv. Mater.* **2010**, *22*, 4355−4358.
(19) Khlyabich, P. P.; Burkhart, B.; Thompson, B. C. *J. Am. Chem. Soc.* **2011**, *133*, 14534−14537.
(20) Shoaee, S.; Subramaniyan, S.; Xin, H.; Keiderling, C.; Tuladhar, P. S.; Jamieson, F.; Jenekhe, S. A.; Durrant, J. R. *Adv. Funct. Mater.* **2013**, 1616−3028.
(21) Mandoc, M. M.; Koster, L. J. A.; Blom, P. W. M. *Appl. Phys. Lett.* **2007**, *90*, 133504.
(22) Shieh, J.-T.; Liu, C.-H.; Meng, H.-F.; Tseng, S.-R.; Chao, Y.-C.; Horng, S.-F. *J. Appl. Phys.* **2010**, *107*, 084503.
(23) Li, G.; Shrotriya, V.; Huang, J. S.; Yao, Y.; Moriarty, T.; Emery, K.; Yang, Y. *Nat. Mater.* **2005**, *4*, 864−868.
(24) Chang, L.; Lademann, H. W. A.; Bonekamp, J.-B.; Meerholz, K.; Moule, A. J. *Adv. Funct. Mater.* **2011**, *21*, 1779−1787.
(25) Zhao, Y.; Xie, Z.; Qu, Y.; Geng, Y.; Wang, L. *Appl. Phys. Lett.* **2007**, *90*, 043504.
(26) Campoy-Quiles, M.; Ferenczi, T.; Agostinelli, T.; Etchegoin, P. G.; Kim, Y.; Anthopoulos, T. D.; Stavrinou, P. N.; Bradley, D. D. C.; Nelson, J. *Nat. Mater.* **2008**, *7*, 158−164.
(27) Treat, N. D.; Brady, M. A.; Smith, G.; Toney, M. F.; Kramer, E. J.; Hawker, C. J.; Chabinyc, M. L. *Adv. Energy Mater.* **2011**, *1*, 82−89.
(28) Treat, N. D.; Mates, T. E.; Hawker, C. J.; Kramer, E. J.; Chabinyc, M. L. *Macromolecules* **2013**, *46*, 1002−1007.
(29) Scharsich, C.; Lohwasser, R. H.; Sommer, M.; Asawapirom, U.; Scherf, U.; Thelakkat, M.; Neher, D.; Koehler, A. *J. Polym. Sci., Part B: Polym. Phys.* **2012**, *50*, 442−453.
(30) Richards, J. J.; Rice, A. H.; Nelson, R. D.; Kim, F. S.; Jenekhe, S. A.; Luscombe, C. K.; Pozzo, D. C. *Adv. Funct. Mater.* **2013**, *23*, 514−522.
(31) Wang, T.; Dunbar, A. D. F.; Staniec, P. A.; Pearson, A. J.; Hopkinson, P. E.; MacDonald, J. E.; Lilliu, S.; Pizzey, C.; Terrill, N. J.; Donald, A. M.; Ryan, A. J.; Jones, R. A. L.; Lidzey, D. G. *Soft Matter* **2010**, *6*, 4128−4134.
(32) Kanai, K.; Miyazaki, T.; Suzuki, H.; Inaba, M.; Ouchi, Y.; Seki, K. *Phys. Chem. Chem. Phys.* **2010**, *12*, 273−282.
(33) Verploegen, E.; Mondal, R.; Bettinger, C. J.; Sok, S.; Toney, M. F.; Bao, Z. *Adv. Funct. Mater.* **2010**, *20*, 3519−3529.
(34) Singh, T. B.; Sariciftci, N. S.; Yang, H.; Yang, L.; Plochberger, B.; Sitter, H. *Appl. Phys. Lett.* **2007**, *90*, 213512.

(35) Wu, W. R.; Jeng, U. S.; Su, C. J.; Wei, K. H.; Su, M. S.; Chiu, M. Y.; Chen, C. Y.; Su, W. B.; Su, C. H.; Su, A. C. *ACS Nano* **2011**, *5*, 6233−6243.
(36) Agostinelli, T.; Lilliu, S.; Labram, J. G.; Campoy-Quiles, M.; Hampton, M.; Pires, E.; Rawle, J.; Bikondoa, O.; Bradley, D. D. C.; Anthopoulos, T. D.; Nelson, J.; Macdonald, J. E. *Adv. Funct. Mater.* **2011**, *21*, 1701−1708.
(37) Gao, D.; Hollinger, J.; Seferos, D. S. *ACS Nano* **2012**, *6*, 7114−7121.
(38) Hollinger, J.; Jahnke, A. A.; Coombs, N.; Seferos, D. S. *J. Am. Chem. Soc.* **2010**, *132*, 8546−8547.